

# Effect of spatial configuration on motion aftereffects

W. L. Sachtler and Qasim Zaidi

*Department of Psychology, Columbia University, New York, New York 10027*

Received July 9, 1992; revised manuscript received January 29, 1993; accepted February 1, 1993

Sensitivity to motion was measured by the percentage of trials on which an observer reported seeing motion of briefly presented high-contrast sinusoidal gratings moving over a range of velocities. The psychometric curve was remeasured following adaptation to a grating moving in one direction for an extended period of time. Adaptation shifted the minimum of the psychometric curve toward the direction of the adapting stimulus. The shift was smaller when the adapting field was larger than the test. In a second set of experiments we measured the effect of motion adaptation on contrast thresholds for moving gratings of different sizes. Threshold elevation was maximal when adapting and test sizes matched. We present a mechanistic model of the motion aftereffect that consists of independent multiplicative gain controls in motion-sensing mechanisms tuned to different rates of motion. In addition, we discuss a model of size effects in motion adaptation that invokes diffuse inhibitory connections among motion-sensing mechanisms.

## 1. INTRODUCTION

After prolonged exposure to a stimulus moving in one direction, observers perceive stationary stimuli to move in the opposite direction. This motion aftereffect has been known since Aristotle described it in his treatise on dreams and has been addressed in many studies.<sup>1-3</sup> Some studies have addressed properties of the motion aftereffect itself, such as its duration and decay,<sup>4,5</sup> and the effect of contrast.<sup>6</sup> A few studies have employed the motion aftereffect in an attempt to gain information about the underlying motion-sensing mechanisms: Pantle<sup>7</sup> estimated the temporal-frequency tuning of motion-sensitive mechanisms from the relative strength of the aftereffect, while other studies focused on differences between color and luminance pathways in the processing of motion information.<sup>8-13</sup>

In more recent studies of the properties of motion-sensing mechanisms, it has been found that contrast thresholds for tests moving in the same direction as an adapting stimulus are elevated more than for tests moving in the opposite direction. Studies have addressed spatial-frequency selectivity,<sup>14-17</sup> orientation tuning,<sup>16,18,19</sup> independence and interaction of mechanisms,<sup>20-22</sup> and temporal tuning.<sup>23,24</sup> One of the drawbacks of this method is that the difference in threshold elevation between opposing directions is rarely more than a factor of 2, so that differences in the magnitude of adaptation across experimental conditions are not easily discernible.

We estimated sensitivity to motion of suprathreshold stimuli by measuring the proportion of trials in which a briefly presented, slowly moving stimulus was seen to move. This was done for several test velocities, the result being a psychometric curve for the detection of motion. The minimum of the curve was at zero velocity. With the same method, we remeasured the psychometric curve after the observer had prolonged exposure to a moving stimulus. Following motion adaptation, the minimum of the curve was no longer at zero but was shifted toward the same direction as the adapting stimulus. Stationary

stimuli appeared to move, as expected from the motion aftereffect, while some stimuli that were physically moving in the adapting direction were rarely seen to move. The velocity to which the minimum of the curve shifts reflects the strength of the motion aftereffect. Following the experimental sections, we present a mechanistic model of the motion aftereffect that generates psychometric curves that fit the experimental data.

We also used this experimental method to study the effect of the size of a moving field on the motion aftereffect. The motion aftereffect and motion adaptation have generally been studied by scrupulously matching the size and location of the adapting and test fields. Spatial phenomena have been addressed primarily in the form of spatial-frequency selectivity or orientation dependency of adaptation. Very few studies have examined the role of spatial configuration in motion perception and adaptation. In general, it is thought that the motion aftereffect is restricted roughly to the retinal region in which the adapting field has been presented, although there is some spread into surrounding areas not directly exposed to the adapting stimulus.<sup>1,25,26</sup> On the other hand, Nakayama and Roberts<sup>27</sup> found that contrast threshold elevation for a thin strip of moving vertical sinusoidal grating was actually less pronounced when the size of an adapting field was increased beyond that of the test field. These studies suggest that spatial configuration may be an important factor in the processing of motion information.

In Experiment 1 we measured the magnitude of the motion aftereffect with the new method. Psychometric curves for the detection of motion were measured before and after exposure to a moving adapting stimulus. Adapting and test stimuli had the same dimensions and consecutively occupied the same region on the retina. In Experiment 2 the adapting stimulus was larger than the test; the magnitude of the motion aftereffect in this condition was compared with that measured in Experiment 1. The effect of increasing the size of the adapting stimulus on motion adaptation was corroborated in Experiment 3 by measurement of direction-selective contrast threshold

elevations for moving stimuli. In addition, we used a range of test sizes to explore size-related adaptation phenomena further. In the final two sections we describe computational models of the motion aftereffect and size-dependent adaptation.

## 2. EXPERIMENT 1: VELOCITY THRESHOLDS FOLLOWING MOTION ADAPTATION

In the first experiment we estimated the magnitude of the motion aftereffect under classical conditions that have been shown to elicit a strong aftereffect. This is the case when adapting and test patterns consecutively occupy the same region of the visual field and are of the same dimensions. Stimuli consisted of high-contrast vertical sinusoidal gratings moving at a constant velocity. Gratings were shown within a horizontal window similar to that shown schematically in Fig. 1(a) below. As a baseline we measured the probability for the detection of motion as a function of velocity under neutral adaptation. We then remeasured the psychometric curve following adaptation with a high-contrast vertical grating moving in one direction for an extended period of time. The change in the psychometric curve was used to infer the effects of motion adaptation.

### A. Equipment and Stimulus Generation

Stimuli were displayed on a Tektronix 690SR television monitor running at a frame rate of 120 Hz, interlaced. The  $512 \times 480$  pixel display subtended  $10.67 \times 10$  degrees of visual angle. The display was driven by an Adage 3000-frame buffer generator that permitted 10-bit specification of the intensity of each gun. A maximum of 256 gray levels could be painted on the screen in one frame. To ensure linearity, we corrected the output of each of the three TV cathode guns with a backtransform by means of a look-up table. Mean color for all conditions was an equal-energy white of 50 cd/m<sup>2</sup>. The equipment described here was used for all experiments in this study.

We created sinusoidal gratings on the screen by filling in sequentially numbered pixels from a color lookup table containing sinusoidally modulated gray-level output values. We drifted gratings by offsetting the starting point at which the color lookup table was read from one frame to the next. All color changes were made during the flyback period so that no artifacts were visible on the screen.

To generate the smoothest possible motion at slow velocities we sometimes had to drift a grating at less than one pixel per frame. A lookup table was generated and filled with luminance output values for a period 100 times the period to be generated on the screen. A sinusoidal grating with the intended period length was produced by sampling every 100th entry of the table. This grating could in effect be drifted by as little as 1/100 of a pixel by offsetting the starting point at which the table was sampled.

### B. Observers

Observer WLS, one of the authors, was emmetropic, tested color normal on the Farnsworth-Munsell 100-hue test, and had extensive experience with psychophysical experiments. Observer SD, who was naïve regarding the outcome of the experiments, was emmetropic and had previous experience with psychophysical experiments.

### C. Stimuli

The stimuli used were achromatic vertical sinusoidal gratings presented within a horizontal window, as shown schematically in Fig. 1(a). Both the adapting and the test gratings were at 95% contrast. Adapting and test gratings were 0.25 deg high and appeared on the same central region on the screen. The rest of the screen and areas 0.5 deg wide to the left and right of the gratings were uniform at mean luminance. Two spatial frequencies were used, 0.4 and 4.0 cycles/deg. Test gratings were always of the same spatial frequency as the adapting gratings. The adapting stimulus drifted to the left at 5 Hz. Velocities of the test stimulus were varied for both leftward and rightward movement. A dark fixation spot of 1.25-arcmin diameter was constantly visible at the center of the screen. The screen was viewed binocularly, and artificial pupils were not used. The distance between the screen and the observer was kept constant at 2 m by means of a fixed forehead and chin rest.

### D. Procedure

For the preadaptation measurements [Fig. 1(a), left-hand schematic] a trial began with a uniform screen at mean luminance. Three equally spaced tones cued the presentation of the test stimulus, which moved at a constant velocity for 75 ms. The screen then immediately returned to a uniform field at mean luminance. The observer's task was to report whether the pattern appeared to move. We used detection of motion as a task, since we were particularly interested in identifying the velocity for which the observer did not report seeing motion. This information would have been lost in a task involving forced-choice determination of direction. The initial phase of the test grating, as well as all velocities and directions, was presented randomly. For preadaptation thresholds the data from three different sessions were pooled, so that each velocity was presented in a total of 100 trials for observer WLS, while 45 trials (collected over 9 sessions) were run for observer SD.

The 75-ms presentation of the test stimulus was shorter than the time needed to initiate pursuit movements,<sup>28</sup> and randomization of test direction countered expectancy effects. The test stimulus moved throughout its presentation time; i.e., it was not stationary before and after the test motion. This effect is similar to opening and closing a shutter behind which a pattern moves at a constant velocity.

The postadaptation motion thresholds [Fig. 1(a), center and right-hand schematics] were measured in separate experimental sessions. A total of 60 trials (20 each in three sessions) were run for each velocity for both observers. The adapting stimulus, moving leftward at 5 Hz, was presented for 10 min to reach a state of maximum adaptation. Thereafter, the adapting stimulus was presented for 5 s before each test presentation to maintain the state of adaptation. The observer fixated the spot at the center of the screen throughout the experiment. A uniform field at mean luminance was presented for 500 ms while three tones signaled the ensuing test presentation. Again, the observer's task was to report whether the high-contrast test pattern appeared to move. This criterion is different from simply stating whether one had the sensation of motion, since that can occur even when one is viewing a uniform field after adapting to motion.<sup>29,30</sup>

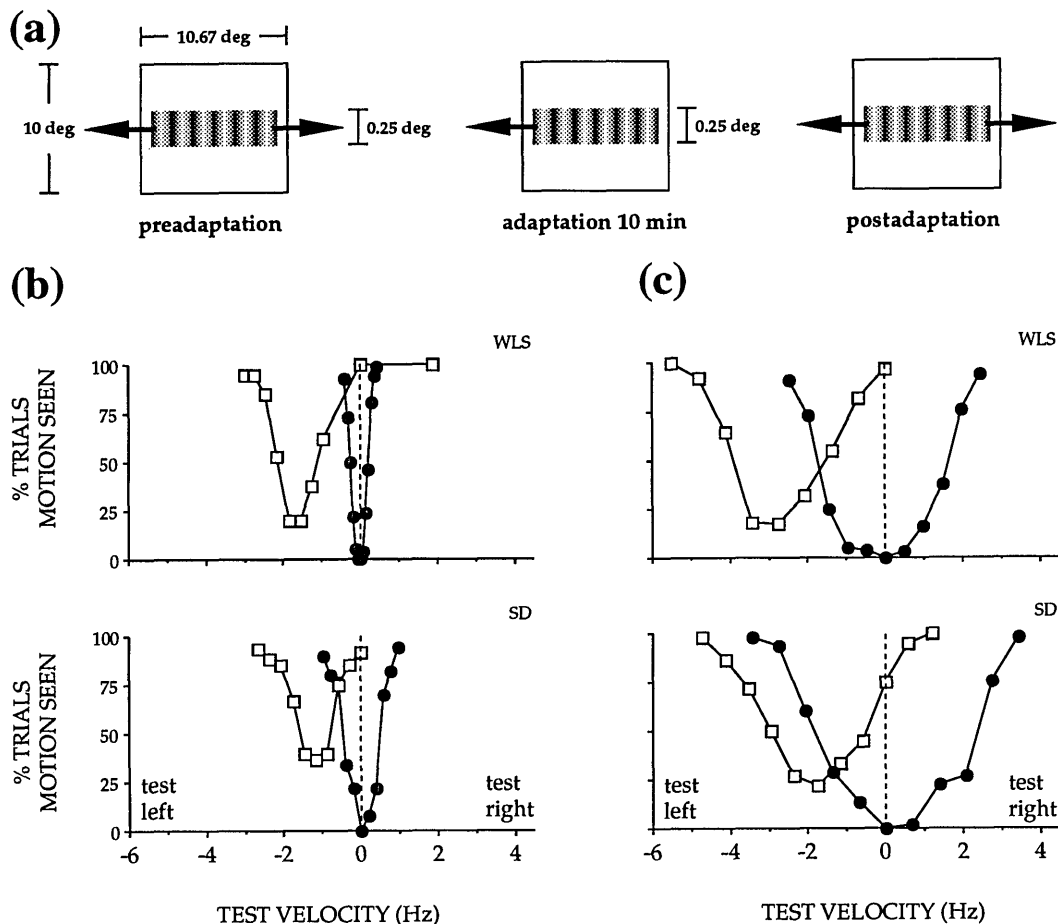


Fig. 1. (a) Stimuli used in Experiment 1. (a) Vertical achromatic gratings at 95% contrast were shown within a thin horizontal window. The remainder of the screen was kept at an equal-energy white of  $50 \text{ cd/m}^2$ . All tests were  $0.25 \text{ deg}$  high. The observer fixated a spot at the center of the screen (not shown here). Gratings were presented for  $75 \text{ ms}$  and moved left or right at a fixed velocity throughout their presentation time. Three tones cued the onset of a trial. The observer adapted to a uniform screen for  $2 \text{ min}$  before trials began in the baseline condition (left-hand panel). The observer's task was to determine whether he had seen the gratings move. In another set of trials, an adapting grating identical to the test grating was presented for  $10 \text{ min}$ , moving leftward at  $5 \text{ Hz}$  (center panel). The observer fixated the spot at the center of the screen. Following adaptation, tests were again presented for  $75 \text{ ms}$  (right-hand panel). Test trials alternated with  $5 \text{ s}$  of top-up adaptation. (b) Results for two observers for gratings of a spatial frequency of  $0.4 \text{ cycle/deg}$ . (c) Results for  $4.0 \text{ cycles/deg}$ . In the cases for both (b) and (c), adapting gratings were of the same spatial frequency as the test gratings. Negative values indicate motion to the left. Filled circles, preadaptation results; open squares, postadaptation results. Lines connect points for clarity and do not have theoretical significance.

For both the preadaptation and the postadaptation measurements we collected data within a restricted range of velocities that covered the psychometric curves as previously determined by a pilot run. The test pattern was stationary on at least 10% of the trials for a given testing condition. The range of test velocities was centered at zero for the preadaptation measurements so that both limbs of the psychometric curve could be measured. Adaptation with a pattern moving to the left elicits a motion aftereffect to the right. Therefore the range of test velocities was shifted toward leftward motion for the posthabituation condition.

### E. Results

Preadaptation velocity thresholds are shown in Fig. 1 as filled circles for two observers. Figure 1(b) shows the results for  $0.4\text{-cycle/deg}$  gratings, and Fig. 1(c) for  $4.0\text{-cycle/deg}$  gratings. The units on the abscissa for each graph are hertz, the temporal rate at which a test pattern was moved during its  $75\text{-ms}$  presentation. The ordinate

gives the percentage of times that an observer indicated that the test pattern appeared to move. The preadaptation psychometric curves for both spatial frequencies are roughly symmetric around zero. The psychometric curves for  $4.0\text{-cycle/deg}$  gratings were wider than the curves for  $0.4\text{-cycle/deg}$  gratings. At zero velocity, the observers did not report seeing motion.

Following adaptation with a  $0.25\text{-deg}$  grating moving to the left, the minima of the psychometric curves for both spatial frequencies were shifted toward leftward test velocities (open squares). Phenomenologically, it is as if tests needed to be moved leftward in order to counteract the apparent rightward movement produced by the motion aftereffect. For observer WLS, stationary tests of  $0.4 \text{ cycle/deg}$  appeared to move in all trials, while tests moving leftward at velocities near  $1.75 \text{ Hz}$  were seen to move in only 20% of the trials. The psychometric curve following adaptation is wider than the preadaptation curve. Furthermore, the left limb of the postadaptation curve resembles the left limb of the preadaptation curve,

while the right limb is shallower after adaptation than the corresponding limb of the curve measured before adaptation. For observer SD the same qualitative descriptions hold, except that the postadaptation curve does not exhibit the asymmetry.

For the 4.0-cycle/deg grating, the minimum of the psychometric curve for observer WLS was at approximately 3.0 Hz of leftward movement of the test. Detection responses around the minimum velocity were between 15% and 20%. The left limb of the postadaptation curve again resembles the left limb of the preadaptation curve, while the right limb of the curve is shallower. For observer SD the effects of adaptation are similar, except that there is no marked asymmetry in the postadaptation curve.

The results of this experiment show that motion adaptation can be measured by the perceived motion of suprathreshold patterns. If a slowly moving stimulus is presented for a long enough time, an observer can infer its motion by remembering its position at the beginning of a trial and comparing that with its position at some later time. Therefore it is important to disentangle sensitivity to motion from acuity for offsets<sup>31</sup> or comparisons of position over time. The results of this experiment indicate that under the present conditions we were in fact measuring thresholds for the detection of motion rather than of offset: following motion adaptation, the curve for the probability of detection of motion was shifted away from zero velocity in the adapting direction. At the minimum of the curve, a moving stimulus was rarely seen to move. On the other hand, a stationary stimulus appeared to move in the majority of trials. It seems unlikely that a positional, or offset, threshold was measured, since it would appear paradoxical that a nonzero displacement should be less detectable than no displacement at all. The shift in the psychometric curves following adaptation is most reasonably explained if sensitivity for velocity were affected. Thus it seems valid to conclude that the psychometric curves reflect the probability of detection of motion rather than of offset.

#### F. Discussion

We have shown above that psychometric curves for the detection of motion are shifted following adaptation with a stimulus moving in one direction. Cords and Bruecke<sup>32</sup> used a similar technique to determine the null-velocity range of the motion aftereffect. They employed two patterned moving belts, which could be viewed alternately when a mirror was moved into the observer's line of sight. After adapting to a moving pattern, the observer viewed the test pattern, which was moving at one of a range of velocities. The observer then judged the direction of motion according to the "first impression" or gave an "undecided" answer when the direction could not be determined clearly. Cords and Bruecke then considered the range of the undecided test velocities as capturing the motion null velocity. Apart from the technical limitations, which included a short period of disrupted fixation as the mirror was swung into place, the criterion based on the first impression would seem ambiguous, since the motion aftereffect decays quickly.<sup>4,5</sup> Cords and Bruecke reported that direction reversals of the apparent movement of the test occurred, so that a first impression might easily have been influenced by the ensuing appearance of the

test. Finally, the range of undecided velocities, for which no unambiguous direction of movement was perceived, was considerable and hid the best motion null. Our method has the advantage that within the short presentation time of the test (75 ms), the motion aftereffect presumably decayed very little, leading to a consistent percept on which to base a decision. The responses to a range of test velocities were plotted, giving a full psychometric curve on velocity nulling thresholds. Also, the short presentation time precluded prolonged exposure to velocities other than the adapting one, thus minimizing the influence of the test on the state of motion adaptation. Bennett and Westheimer<sup>33</sup> measured adaptation effects on apparent motion, using a technique that shares some features with ours.

More recently, Sekuler and Pantle<sup>4</sup> and Pantle<sup>7</sup> used a technique for determining the velocity of the motion aftereffect in which they compared an estimate of the magnitude of the apparent velocity of a stationary test pattern with a previously seen standard velocity. This method was considered to be less obtrusive than the motion null used by Cords and Bruecke, since no moving tests were presented that could have interfered with the state of motion adaptation. The magnitude-estimation task has the disadvantage that the observer is required to retain a standard velocity in memory, with the possibility of a criterion shift's taking place during the course of an experiment. In our experiments the observers merely had to decide whether the test appeared to move, which is a simpler decision without memory requirements. In addition, our method generates a full psychometric curve that gives information about motion sensitivity, whereas magnitude estimation gives just one data point.

The changes in the psychometric curve following motion adaptation put constraints on the types of model that can be invoked to explain the motion aftereffect. Following the sections that describe our experiments, we present a model that meets these constraints (Section 5).

### 3. EXPERIMENT 2: EFFECTS OF FIELD SIZE ON MOTION ADAPTATION

We employed the new method to study some spatial properties of adaptable motion-sensing mechanisms by increasing the height of the adapting gratings while test gratings remained the same [Fig. 2(a)]. In this experiment, adapting and test stimuli differed only in the vertical dimension, orthogonal to the direction of motion, and were identical along the direction of motion.

#### A. Stimuli

Stimuli used were achromatic vertical sinusoidal gratings presented within horizontal windows, as shown schematically in Fig. 2(a). Both the adapting and the test gratings were at 95% contrast, consecutively appearing, and centered on the same region on the screen. All test gratings were 0.25 deg high, while adapting gratings were 9.0 deg high. For ease of description we refer to the 0.25- and the 9.0-deg gratings as short and tall, respectively. Again, two spatial frequencies were used, 0.4 and 4.0 cycles/deg, and test gratings were always of the same spatial frequency as the adapting gratings. The adapting stimulus was drifted to the left at 5 Hz.

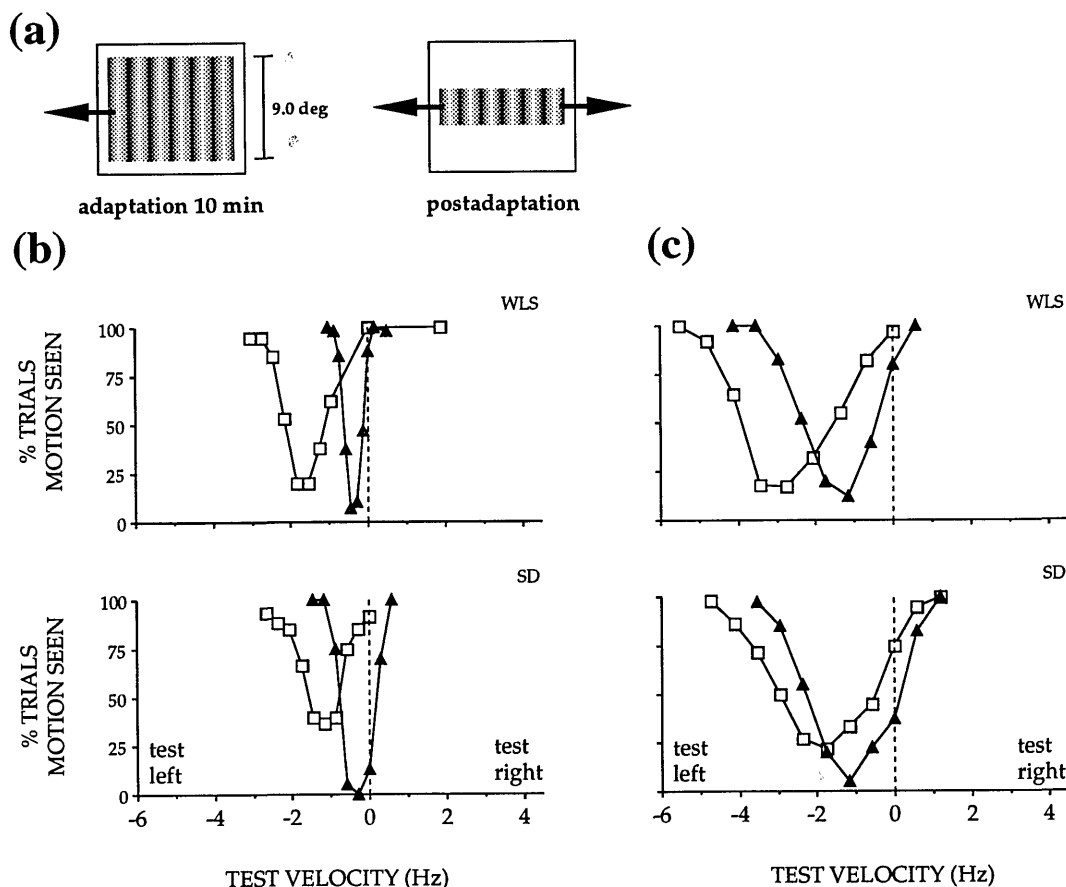


Fig. 2. (a) Stimuli used in Experiment 2. (a) Postadaptation tests were 0.25 deg high, as in Experiment 1. The adapting grating was 9.0 deg high. Results for gratings of (b) 0.4 and (c) 4.0 cycles/deg. Filled triangles, results for tests 0.25 deg high following adaptation with a grating 9.0 deg high. For comparison, results from Experiment 1 (adapting and testing with gratings 0.25 deg high) are shown again as open squares.

## B. Procedure

Postadaptation velocity thresholds were measured in three experimental sessions for a total of 60 trials for each test velocity for observer WLS and for 40 trials for observer SD. The adapting stimulus, moving leftward at 5 Hz, was presented for 10 min, during which the observers fixated the spot at the center of the screen. Thereafter, each test presentation was preceded by 5 s of top-up adaptation. A uniform field at mean luminance was presented for 500 ms while three tones signaled the ensuing test presentation. The observers' task was again to report whether the pattern appeared to move.

## C. Results

The results for adapting with a tall grating and testing with a short grating are shown in Figs. 2(b) and 2(c) (filled triangles) for gratings of 0.4 and 4.0 cycles/deg, respectively. For comparison, the results of adapting and testing with a short grating are shown again as open squares. For the 0.4-cycle/deg grating, the minimum of the psychometric curve was at approximately 0.4 Hz of leftward movement for observer WLS, with motion being perceived between 5% and 10% of trials around that velocity. The psychometric curve following adaptation with the tall grating was displaced less than the curve following adaptation with the short grating and did not widen markedly. Results were qualitatively similar for observer SD.

The minimum of the psychometric curve for the 4.0-cycle/deg grating was at approximately 1.3 Hz for observer WLS, with motion being perceived in 12% of trials. Again, the psychometric curve was displaced less than after adaptation with the short grating. The psychometric curves following adaptation with a tall or a short grating were narrower than the preadaptation curve. Results were qualitatively similar for observer SD.

Even though the short test field was completely within the area covered by the tall adapting field, it was adapted less than by a field its own size. When adaptation was with a tall field, the upper and lower boundaries of the adapting and test fields no longer coincided, and the overall area of the moving adapting stimulus was larger.

These results cannot be explained in terms of independent early motion-sensing mechanisms that have been proposed.<sup>34-36</sup> These models of motion-sensing mechanisms generally invoke some form of spatial receptive field within which stimulus inputs are summed. The responses of such mechanisms depend on the degree of coverage of the receptive field for an otherwise optimal stimulus: output is maximal when the receptive field is completely covered by the stimulus and does not change if the stimulus size is increased further. The tall adapting grating would therefore be expected to adapt these types of motion-sensing mechanism at least as much as does the short grating. Since the magnitude of motion adaptation

was *reduced* when the adapting grating was of a larger spatial extent than the test, an explanation of the results requires some form of spatial interaction across such mechanisms.

In Experiment 3 we replicated the results of Experiments 1 and 2 for motion adaptation by measuring threshold contrast for the detection of moving gratings. In addition, we further explored the relationship between adapting and test size to determine whether tall adapting gratings were simply less effective than short gratings in eliciting motion adaptation.

#### 4. EXPERIMENT 3: CONTRAST THRESHOLD ELEVATION FOR MOVING SINUSOIDAL GRATINGS FOLLOWING MOTION ADAPTATION

Since the results of Experiments 1 and 2 were obtained with a new method, we repeated the experiments, using one of the more commonly used methods for measuring motion adaptation. We compared the contrast threshold at which moving gratings were detected before and after exposure to the adapting stimulus. Sekuler and Ganz,<sup>37</sup> using a stabilized retinal image, found direction-selective contrast-threshold elevation for moving patterns following exposure of observers to a high-contrast moving stimulus. Later studies found the effect to be robust under nonstabilized viewing conditions.<sup>18,23,28</sup> The methods used in Experiment 3 were similar to the ones used in those studies. An observer fixated a small spot while being presented with a uniformly moving high-contrast grating for an extended period of time. Following that, a moving low-contrast test grating was presented, and the observer indicated whether he had seen it.

In addition to replicating Experiments 1 and 2, we further explored the effect of the relationship between adapting and test sizes on motion adaptation. For this, we used the tall adapting grating and varied the size of the test gratings.

##### A. Stimuli

Stimuli consisted of vertical sinusoidal gratings presented within windows of various heights. Adapting fields were gratings of the same spatial frequency as the test gratings. The center of the adapting grating coincided with the center of the test field. There was a 0.5-deg-wide uniform border at mean luminance around the edges of the gratings. In the first condition, both adapting and test fields were 0.25 deg high. In the remaining conditions, the adapting field was 9.0 deg high, and tests were 0.25, 1.0, or 9.0 deg high. Schematics of the stimuli are shown as abscissa labels in Fig. 3. Adapting gratings were at 95% contrast. We varied the contrast of the test gratings to determine contrast threshold. Again, two spatial frequencies were employed, 0.4 and 4.0 cycles/deg. Adapting gratings were drifted leftward at 5 Hz for 10 min. Test gratings were presented for 1 s drifting left or right at the same velocity, followed by 5 s of top-up adaptation.

##### B. Procedure

Preadaptation contrast thresholds were measured independently for rightward and leftward motion of the test stimulus, which was presented for 1 s following three

evenly spaced cueing tones, and test directions were randomized. Following 10 min of adaptation with the leftward-moving adapting field, contrast thresholds were again determined for both directions of movement of the test stimulus. Thereafter, each test presentation was preceded by 5 s of top-up adaptation. Since the adapting grating was at 95% contrast, while the test grating was always near threshold, the two were easily discriminable. Furthermore, the test was presented for 1 s. Therefore no cueing tones were used, and the test simply followed the adapting stimulus immediately. A tone signaled the end of the test presentation. Thresholds were determined with an interleaved double-random staircase tracking the 80% detection point.<sup>39</sup> Six transitions were run for each staircase, so that each data point is the mean of 12 values.

##### C. Results

We have calculated two indices of desensitization from each set of contrast thresholds. The first index reflects the total desensitization, where thresholds for tests moving in the same direction as the adapting grating were compared before and after adaptation.<sup>23,40</sup> This index was calculated as follows:

total desensitization

$$= \log \left[ \frac{\text{threshold (postadapt same direction)}}{\text{threshold (preadapt same direction)}} \right]. \quad (1)$$

Positive values of this index indicate threshold elevations for tests moving in the direction of adaptation. This index is plotted as open circles in Figs. 3(a) and 3(b).

The second index reflects directional desensitization, where thresholds following adaptation were compared for tests moving in the same direction as the adapting stimulus and for tests moving in the opposite direction.<sup>38,40</sup> This index was calculated as follows:

directional desensitization

$$= \log \left[ \frac{\text{threshold (postadapt same direction)}}{\text{threshold (postadapt opposite direction)}} \right]. \quad (2)$$

Positive values of this index correspond to greater desensitization in the direction of adaptation than in the opposite direction. This index is plotted as filled squares.

Results for gratings with spatial frequencies of 0.4 and 4.0 cycles/deg are shown in Figs. 3(a) and 3(b), respectively, for two observers. The adapting and testing configurations are shown for each condition at the bottom of the figure. Desensitization indices for adapting and testing with a grating 0.25 deg high are shown in the left-hand columns of Figs. 3(a) and 3(b). When the adapting grating was 9.0 deg high, thresholds for the 0.25-deg test were not elevated so much, as is shown by lower desensitization indices in the second column. For observer WLS, both measures of motion adaptation decrease in magnitude as the size of the adapting grating is increased beyond that of the test. For observer SD, the index for total desensitization, which partially reflects non-direction-selective contrast-threshold elevation, shows some irregularity. The directional desensitization index, though, is quite systematic across all conditions.

In the third and fourth columns we show results for adaptation with a grating 9.0 deg high when test gratings were 1.0 and 9.0 deg high, respectively. As test size was

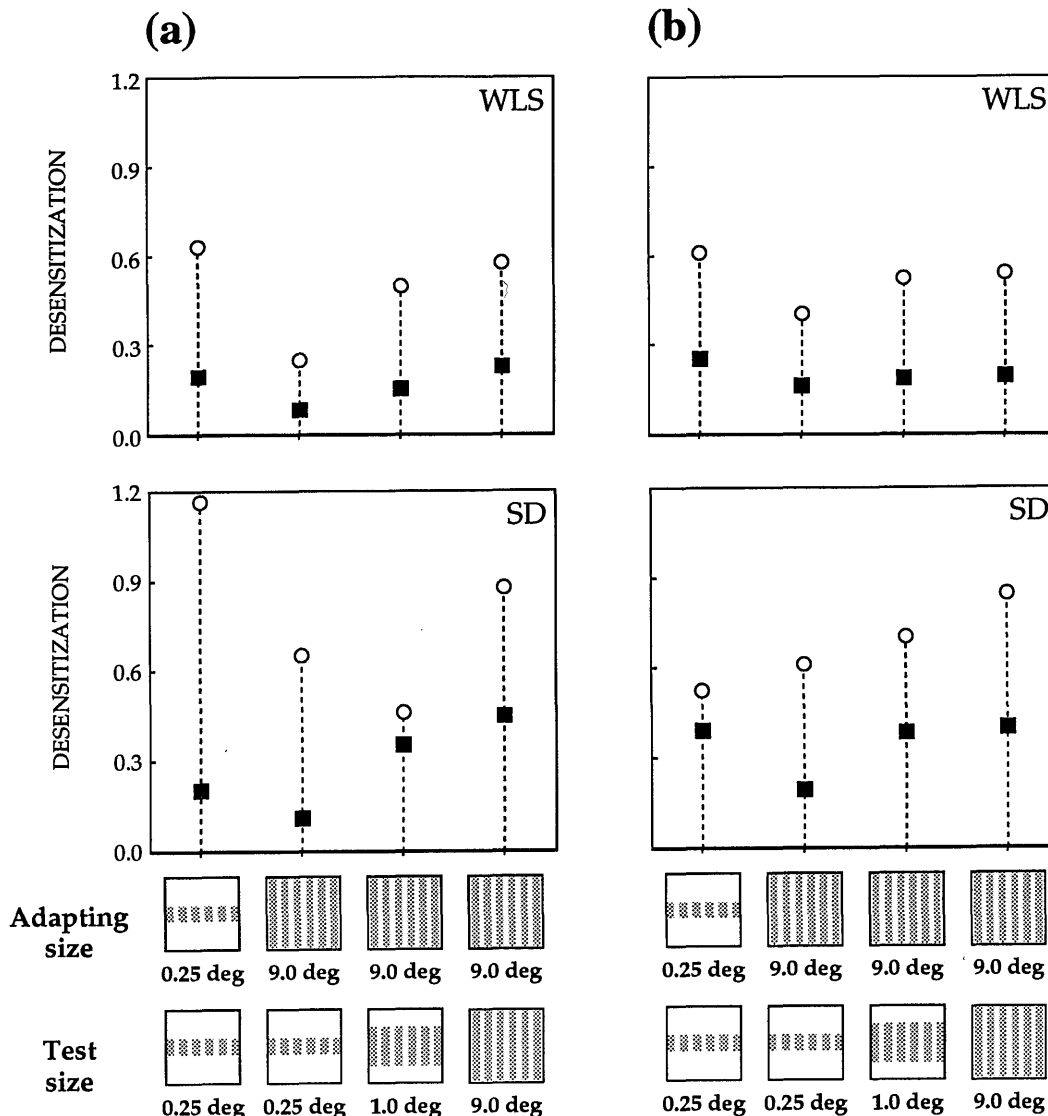


Fig. 3. Results of Experiment 3. Tests were presented for 1 s, moving leftward or rightward at 5 Hz. We varied the contrast of the gratings to determine contrast threshold for detection of the moving gratings. Results for two observers for (a) 0.4-cycle/deg gratings and (b) 4.0-cycle/deg gratings. The abscissas are divided into the four experimental conditions tested. The particular adapting and test-size configurations for each category are shown below the graphs. Desensitization indexes plotted on the ordinate reflect the amount of contrast threshold elevation following adaptation with a grating at 95% contrast. The total desensitization index compares contrast thresholds for tests moving in the same direction as the adapting grating before and after adaptation [see Eq. (1)]. Positive values indicate that thresholds were elevated following adaptation (open circles). The index of directional desensitization compares postadaptation thresholds for the two test directions [see Eq. (2)]. Positive values indicate that thresholds for tests moving in the same direction as the adapting grating were elevated more than thresholds for tests moving in the opposite direction (filled squares).

increased, the magnitude of desensitization increased also. Adaptation was maximal when both the adapting and the test fields were 9.0 deg high. Thus the overall pattern is that motion adaptation is less pronounced when adapting and test sizes differ, while it is maximal when the sizes match.

#### D. Discussion

These results extend the findings of Nakayama and Roberts,<sup>27</sup> who showed that contrast-threshold elevation was less pronounced when the adapting field size was increased beyond the size of the test. Using the contrast-threshold-elevation paradigm, we showed in addition that threshold elevation was again more pronounced when test sizes were increased to match a tall adapting field.

Nakayama and Roberts suggested that motion information about short and tall fields is processed by different sets of mechanisms tuned to varying sizes. We suggest that a model in which mechanisms interact through diffuse inhibitory connections whose strength decreases with distance would also be consistent with the data. In this model the output of mechanisms exposed to the interior of a large moving stimulus is reduced. Mechanisms near the edges of the stimulus receive less inhibition, so their output is greater. Adaptation takes place independently within each mechanism and occurs after the inhibitory inputs from surrounding mechanisms are pooled. Mechanisms near the center of a large adapting stimulus will adapt less than those near the edges. Thresholds for a small test centered on the same retinal region as a large

adapting stimulus therefore will be less elevated. Preadaptation thresholds for large tests will be determined by the responses of mechanisms near the edges of the stimulus, since these have the greatest output. During adaptation, the response of these mechanisms is reduced the most. Thresholds are elevated following adaptation, since outputs of the formerly most responsive units near the edges of the stimulus are reduced. We present a formal version of this model in Section 6.

## 5. MODEL OF THE MOTION AFTEREFFECT

In this section we present a model of the motion aftereffect. The psychometric curves generated by this model for the probability of detection of motion for tests at different velocities were fitted to the preadaptation and postadaptation 4-cycle/deg results of Experiment 1 for observer WLS.

Even though a large number of experimental studies on the motion aftereffect have been published,<sup>1-3</sup> only a few have attempted quantitative modeling. Wohlgeuth<sup>1</sup> proposed that the motion aftereffect could be due to a mechanism subjected to some form of neuronal fatigue following prolonged exposure to a moving stimulus. Sutherland<sup>41</sup> and Clymer<sup>42</sup> assumed that adaptation fatigues one member of an opponent pair of mechanisms, thus creating an imbalance of outputs. The idea at the core of Sutherland's suggestion has been applied to experimental results only as a verbal description,<sup>1,4,42,43</sup> and no one has attempted to fit experimental data with a mathematical model. This lack of explicit models may be due in part to a lack of knowledge about the motion-sensing mechanisms themselves and in part to a lack of quantitative data that lend themselves to modeling of the motion aftereffect. Until recently the most common measures of the motion aftereffect were decay time, for which a tracking or continuous nulling technique was used; estimated magnitude; and velocity matching across retinal locations.<sup>4,5,7,42,43</sup> Although there is some consensus about models of early mechanisms that sense motion,<sup>34-36</sup> the extraction of the velocity of a moving stimulus from the signals of these early mechanisms is still an unresolved problem. Thus data based on the estimated magnitude of the motion aftereffect and on velocity matching, i.e., estimates of the apparent velocity of a test stimulus, are of limited use for modeling of the motion aftereffect because of a lack of knowledge about the extraction of velocity information from the signals of early motion-sensing mechanisms.

The types of data collected by the experimental methods used in this study are easier to model, even though it is still necessary to make a number of linking assumptions. The data from our experiments consist of complete psychometric curves of the probability of detection of motion. This is advantageous for modeling, since it requires only a general model of motion-sensing mechanisms whose outputs are passed through a function that directly generates probabilities of detection. Thus, later stages of the motion system for disentangling stimulus contrast and velocity are not needed, as they can be assumed to be largely transparent to stimuli moving at threshold velocities. In this section we focus on a model of the motion aftereffect in the case in which adapting and test fields are of the same dimensions.

The core of the model is a variant of the spatiotemporal-energy model proposed by Adelson and Bergen.<sup>36</sup> In this model, the visual scene is sampled with a set of phase-shifted spatiotemporal filters whose outputs are transformed and combined in such a way as to produce two channels preferentially tuned to opposite directions of motion. The outputs of the two channels are then subtracted from one another to yield a value,  $M$ , whose sign reflects the direction of motion. Verbal descriptions of models for the motion aftereffect seem to refer exclusively to such opponent processes.<sup>41</sup> In fact, there appears to be little evidence for exclusively bidirectional opponent-motion mechanisms.<sup>44</sup> In a more general model, the outputs of channels tuned to various orientations and directions of motion could be combined, in effect providing a vector sum of motion energies in different directions. This kind of model could explain results, including those for the motion aftereffect, for which a simple opponent stage has been proposed. In the present experiments, motion was confined to the two opposite directions along one spatial axis. Therefore we have found it sufficient to use only mechanisms tuned to these two directions. The results of this study do not themselves endorse an opponent stage of motion processing. We have used the Adelson-Bergen model instead of other models because of the ease of manipulating the preopponent mechanisms in this model.

In order to introduce adaptation properties to the model, we added independent multiplicative gain-control

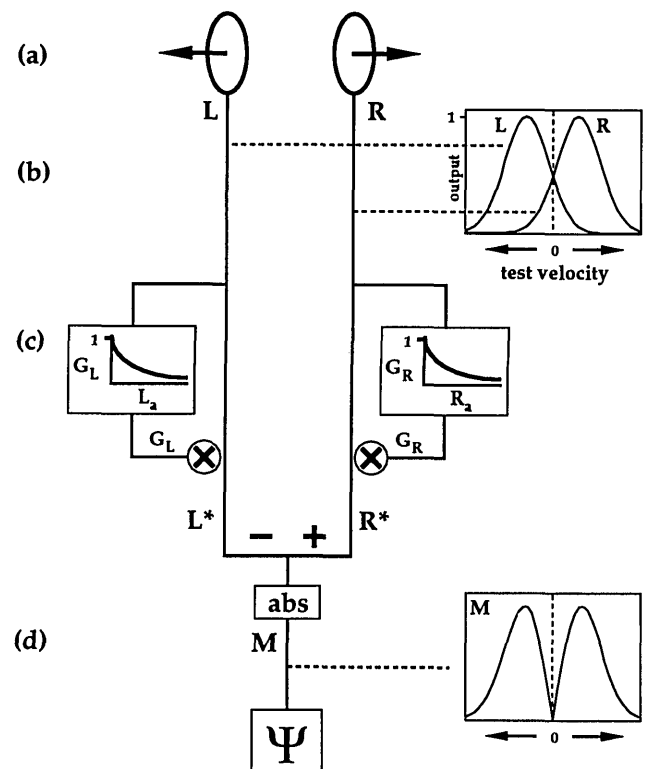


Fig. 4. Schematic of a motion-sensing mechanism with adaptable properties whose output is used to generate probabilities of detection for gratings moving at different velocities. (a) Spatiotemporal filters tuned to leftward (L) and rightward (R) motion, (b) output of L and R channels as a function of the speed and direction of a moving grating, (c) independent multiplicative gain-control mechanisms for L and R channels. (d) The absolute value of the opponent output  $M$  is fed into a function,  $\Psi$ , which generates a probability of detection of motion.

mechanisms for the leftward- and rightward-sensitive channels before the opponent combination. A schematic of the model is shown in Fig. 4. The outputs of the leftward- and rightward-sensitive channels shown in Fig. 4(a) are labeled L and R, respectively. The responses of subunits preferentially tuned to leftward and rightward motion are shown schematically in Fig. 4(b), at the right. The velocity-response curves shown in the diagram reflect the outputs of tuned spatiotemporal filters as a function of the velocity of sinusoidal gratings. The L channel responds maximally to leftward movement of a particular temporal frequency. Its output decreases for frequencies higher or lower than the optimal value. The spatiotemporal filters proposed by Adelson and Bergen give a steady output to moving sinusoidal gratings. An important property of the tuned spatiotemporal filters is that they do not give zero output when exposed to a stationary pattern. In fact, each filter responds to movement even in the nonpreferred direction. This is apparent from the description of motion-sensing mechanisms as orientable filters in space and time.<sup>36</sup> Complex cells in cat striate cortex have been shown to have similar properties.<sup>44</sup> The functional form of the velocity-response curves chosen for our model is a Gaussian; the location of the peak of the curve on the frequency axis is the optimal test velocity. The actual shape of the curve, which depends on the particular temporal filters used, is not critical to the functioning of our model. It is relevant only that there be a preferred direction of motion, with a decline in output for lower velocities, and nonzero responses to stationary stimuli and to motion in the nonpreferred direction.

In the model, prolonged exposure to a moving stimulus affects multiplicative gain-control mechanisms, as shown schematically in Fig. 4(c). The gain values for the L and R channels are calculated according to the following formulas:

$$G_L = \frac{k}{k + (L_a)^p}, \quad (3)$$

$$G_R = \frac{k}{k + (R_a)^p}, \quad (4)$$

where  $L_a$  and  $R_a$  are the outputs of the L and R channels during adaptation and  $k$  is a constant that is the same for both channels. The exponent  $p$  can be used to modify the input to the gain function and is set equal to one in this model. The gain functions return values between zero and one. The greater the output of a channel during adaptation, the smaller the corresponding gain value. The outputs produced in the L and R channels in response to a moving test stimulus are multiplied by the corresponding gain values:

$$L^* = L * G_L, \quad (5)$$

$$R^* = R * G_R. \quad (6)$$

In the model we assume that the gain values before adaptation are both equal to one. Therefore, before adaptation,  $L^* = L$ , and  $R^* = R$ .

The output of one channel is then subtracted from that of the other channel to yield a value whose sign reflects the direction of motion. Since the results of our experiments were based on the detection of motion irre-

spective of direction, we considered only the absolute value of the opponent response in our model:

$$M = |R^* - L^*|. \quad (7)$$

This is shown schematically in Fig. 4(d), where curve  $M$  is the absolute value of the difference between curves L and R in Fig. 4(b).

In order to relate the opponent output to probability of detection, we used the Quick<sup>45</sup> psychometric function:

$$\Psi = 1 - \prod_{i=1}^N [1 - (1 - 2^{-\mathcal{R}_i/\alpha})], \quad (8)$$

where  $\mathcal{R}_i$  is the normalized response of mechanism  $i$  found by dividing the response  $M_i$  by a factor,  $m$ . The parameter  $m$  determines the velocity at which detection equals 50% for a single mechanism. This function serves to calculate the probability of detection following probability summation of several channels. The exponent  $\alpha$  is a parameter used to vary the slope of the psychometric curve, and  $N$  is the number of mechanisms pooled.

In this model we assume that, at the time of testing, adaptation has reached a steady state and is not altered significantly by the presentation of the tests. This appears to be reasonable, since in our experiments we initially adapted for 600 s and interleaved tests with 5-s top-up adaptation, whereas tests were presented for only 0.075 s. To simplify the modeling, we assume that the presentation of a test was long enough to allow the spatiotemporal filters to reach steady-state output. It is questionable whether this would be possible given the 75-ms test in our experiments, but it seems plausible that the velocity-response curve for a test of short duration will have a functional form similar to that for a longer test.

In Fig. 5 we apply the model in a first attempt to fit the data of Experiment 1, in which we measured psychometric curves for the detection of motion before and after prolonged exposure to a stimulus moving in one direction. Preadaptation and postadaptation results are shown in the left- and right-hand columns, respectively. Test velocities are plotted on the abscissas in hertz. We employed only one motion-sensing mechanism tuned to 5 Hz ( $\sigma_{\text{mech}} = 3$  Hz); this value corresponds to the velocity of the adapting stimulus in the experiments. The velocity-response curves for the constituent spatiotemporal filters are shown in Fig. 5(a). The height of the Gaussian response curves was set to 8 units. The adapting stimulus moved leftward at 5 Hz, indicated by an arrow, labeled a, in the left-hand graph in Fig. 5(a). The L channel gives a greater response to the adapting stimulus than does the R channel. These are the response values of  $L_a$  and  $R_a$  used to set the gain factor. For this case, the gain constant  $k$  was set to 1.93. The graph at the right shows the response curves following adaptation. The response of the L channel has been reduced by a greater amount than that of the R channel.

The absolute value of the postopponent response for the same range of test velocities is shown in Fig. 5(b). Before adaptation the opponent response to a stationary stimulus is zero. Following adaptation a stationary stimulus elicits a greater response from the R channel, so that the opponent output is not zero: the minimum of the postadaptation curve is shifted to the left. A test stimulus has to be

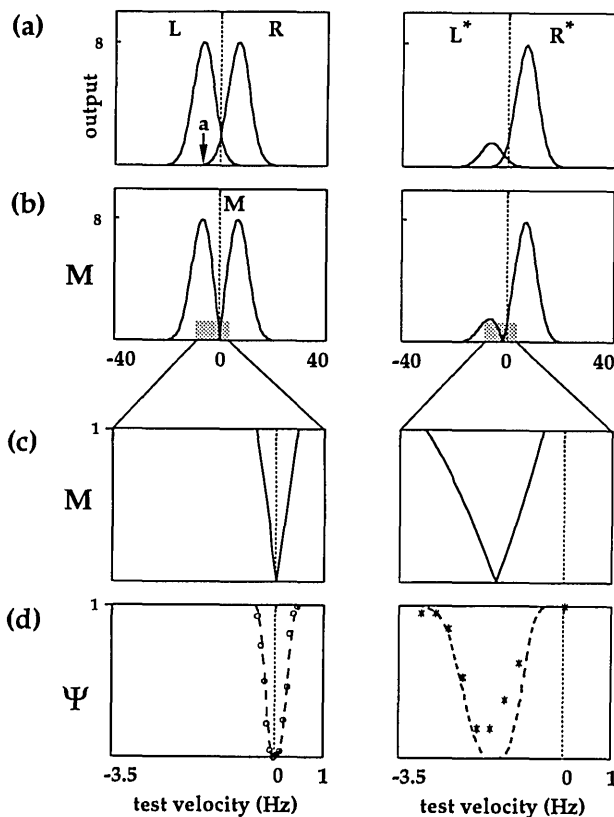


Fig. 5. Application of the model with the use of one set of spatiotemporal filters tuned to 5 Hz. Panels show responses at different stages of the model shown in Fig. 4. Left-hand column, preadaptation responses; right-hand column, corresponding postadaptation responses. Adapting and test gratings were assumed to be the same size, as in Experiment 1. (a) Output of the spatiotemporal filters in response to gratings at 100% contrast, moving at different velocities. The arrow labeled *a* indicates the point on the abscissa that corresponds to the adapting grating moving leftward at 5 Hz. The responses of the L and R channels to that velocity are used to set the gain values. (b) Absolute value of the opponent response. (c) Close-up of the shaded region in (b); the scale on the abscissa changes accordingly. (d) The value of *M* is fed into the Quick psychometric function [see Eq. (8)], producing a probability of detection. Open circles, preadaptation psychometric curve for the detection of motion of 0.4-cycle/deg gratings measured in Experiment 1 for observer WLS; asterisks, experimental results following adaptation. See text for model parameter settings.

moved leftward in order for the L and R responses to be canceled out.

Figure 5(c) gives an enlarged view of the shaded region in Fig. 5(b). The range of test velocities in Figs. 5(c) and 5(d) is the  $-3.5$ -to- $1$ -Hz portion of the  $-40$ -to- $40$ -Hz range in Figs. 5(a) and 5(b). Following adaptation, the response curve for *M* shifts to the left. The values of *M* were passed through the Quick psychometric function to generate curves representing the probability of detection of motion, shown in Fig. 5(d). The parameters were chosen to give a good fit to the preadaptation data ( $m = 0.55$ ;  $\alpha = 3.1$ ). The results from Experiment 1 are shown as circles for the preadaptation condition and as asterisks for the postadaptation measurements.

This simple model captures one key property of the data: following adaptation to the left, the detection curve shifts to the left. What the model does not capture is the nonzero probability of detection at the minimum point of

the postadaptation curve. Also, the left-hand side of the curve generated by the model is shallower than the right-hand side, which is not consistent with the data. These problems can be addressed if one considers the responses from a distribution of mechanisms.

So far we have considered only the responses of a set of mechanisms tuned to one temporal frequency. Electrophysiological recordings in cats and monkeys show that cells can vary in their preferred velocities<sup>46-48</sup> and that the bandwidth of response tends to scale with the preferred velocity. Thus it seems reasonable to assume in the model that there are a number of mechanisms, each tuned to a different preferred velocity. In this case we employed only two sets of mechanisms, as shown schematically in Fig. 6. One set of filters was tuned to leftward and rightward motion at 5 Hz ( $\sigma_{\text{mech}} = 3$  Hz), as described previously in the model shown in Fig. 5. These filters are labeled  $L_1$  and  $R_1$  in Fig. 6. A second set of filters was tuned to motion at 16 Hz ( $\sigma_{\text{mech}} = 11.5$ ), a value chosen to give a good fit to the data. These filters are labeled  $L_2$  and  $R_2$ . These two sets of mechanisms are independent. Their final outputs,  $M_1$  and  $M_2$ , are then pooled by probability summation in the probability function. The responses of the spatiotemporal filters are shown superimposed in Fig. 7(a). The solid curves, labeled  $L_1$  and  $R_1$ , show responses of the subunits preferentially tuned to 5 Hz, while the dashed curves, labeled  $L_2$  and  $R_2$ , show responses of the subunits with peak sensitivity at 16 Hz. Subunit  $L_1$  responds maximally to an adapting grating moving leftward at 5 Hz. The response of subunit  $L_2$  to the same adapting grating is not so pronounced, since its peak response is at 16 Hz. Therefore subunit  $L_2$  will not be adapted quite so much as subunit  $L_1$ . In either case, the outputs of the channels tuned to leftward motion are reduced more than those of the rightward-sensitive channels, as shown in the right-hand panel of Fig. 7(a). The gain constant *k* and parameters for the probability function were the same as in the model shown in Fig. 5. The opponent outputs are shown in Fig. 7(b). Before adaptation both  $M_1$  and  $M_2$  are centered at zero. Curve  $M_2$  is shallower than curve  $M_1$  around zero. Following adaptation, the curves shift by different amounts: curve  $M_2$  shifts farther than curve  $M_1$ . The point at which the Gaussian response curves cross determines the minimum

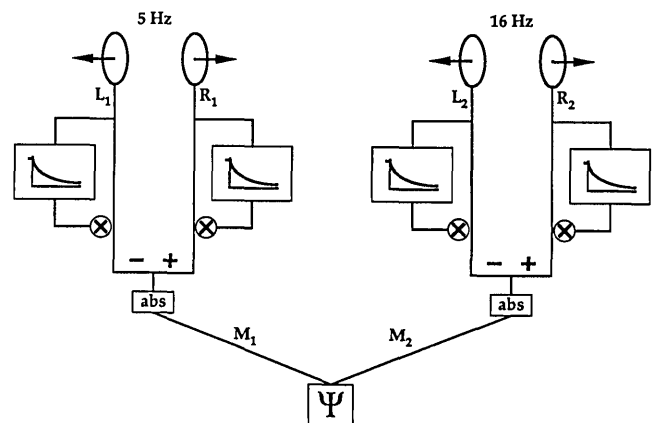


Fig. 6. Expanded model that encompasses independent motion-sensing mechanisms preferentially tuned to different temporal rates. The absolute value of the opponent output is then pooled by means of probability summation in the psychometric function.

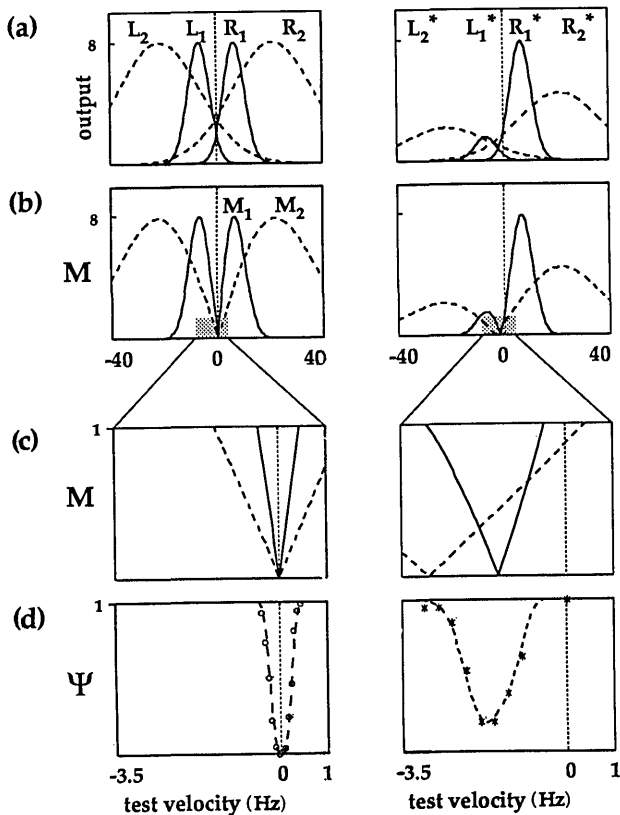


Fig. 7. Application of the model with the use of two sets of independent spatiotemporal filters. Left-hand column, preadaptation responses; right-hand column, postadaptation responses. (a) Solid curves, responses of filters tuned to 5 Hz; dashed curves, those of filters tuned to 16 Hz. (b) Absolute values of opponent responses of the two sets of mechanisms. (c) Close-up of shaded region in (b). (d) Curves  $M_1$  and  $M_2$  are combined through probability summation into one curve that gives probability of detection of moving gratings (dashed curve). Circles and asterisks show the preadaptation and postadaptation results, respectively, for the detection of motion of 0.4-cycle/deg gratings measured in Experiment 1 for observer WLS.

of the opponent response curve. When the height of one of the Gaussian curves is reduced by a constant factor, the shift of the crossing point depends on the slopes of the curves. The greater the standard deviation of the Gaussians, the greater the shift in the crossing point.

Figure 7(c) shows an enlargement of the shaded region in Fig. 7(b). The range of velocities on the abscissa changes accordingly. Results of Experiment 1 are shown in Fig. 7(d) together with the psychometric curves predicted by the model, shown as a dashed line in each panel. Before adaptation (left column), the probability of detection depended primarily on the response of  $M_1$ , which corresponds to the activity of the spatiotemporal filters tuned to lower temporal frequencies. Following adaptation, the probability of detection is also heavily influenced by the response of  $M_2$ . Thus the left-hand side of the curve is determined primarily by  $M_1$ , while the right-hand side is determined primarily by  $M_2$ , which has a shallower slope.

Figure 7(d) shows that this model reflects the data's properties quite well:

1. Following adaptation to the left, the curve for the probability of detection of motion shifts to the left.

2. At the minimum of the curve, the probability of detection is not zero.
3. The slope on the left-hand side of the postadaptation curve is similar to the preadaptation slope, while the slope on the right-hand side is shallower.

These properties were captured with a few simple modifications of an existing class of motion-sensing models:

1. There are several mechanisms tuned to different rates of motion; bandwidths scale approximately with the preferred temporal frequency.
2. Independent multiplicative gain controls affect each channel before the opponent stage.
3. There is probability summation across mechanisms tuned to different rates of motion.

The parameters of the model were chosen arbitrarily to give a good fit to the preadaptation data. For modeling the effects of adaptation, the parameters were kept fixed, and only the gain constant  $k$  was manipulated to produce the appropriate amount of shift in the postadaptation curve.

The model can account for the opening of the postadaptation curve to the right, as was found for observer WLS. In addition, parameters can be chosen to produce very little change in the shape of the curve. A model employing only units tuned to one velocity predicts an opening of the curve to the left, which is not consistent with the data of either observer.

Since the postadaptation psychometric curve for 4.0-cycle/deg gratings is wider, and is shifted more, than the curve for the 0.4-cycle/deg gratings, it cannot be fitted with the use of the same parameters. The model is limited by the scaling properties of the Gaussian response curves. When the difference in scaling between the data sets for the two spatial frequencies is taken into consideration, the model can also generate psychometric curves to match those of the 4.0-cycle/deg data.

A model that seems reasonable at first glance but that will not work is one of independent multiplicative gain controls on channels that respond only to the preferred direction of motion and that give no response for stationary stimuli or for stimuli moving in the nonpreferred direction. Preadaptation curves for the L and R channels of this model are shown schematically in the left-hand panel of Fig. 8(a). The absolute value of the opponent response is shown in the left-hand panel of Fig. 8(b). Following adaptation with a leftward-moving stimulus, the output of the L channel is reduced, as shown at the right in Fig. 8(a). The opponent output after adaptation [Fig. 8(b), right] shows that the response curve becomes shallower in the direction of adaptation and does not shift. This is quite contrary to the experimental results.

We have not found any references to prior efforts at fitting experimental data on the motion aftereffect with an explicit model. Even though our model is based on a general class of motion-sensing mechanisms whose properties have been examined in some detail, it is possible that some other models may produce similar results. In particular, the model described in this section is based on independent multiplicative gain controls before the opponent stage. It is possible that a subtractive adaptive mechanism after

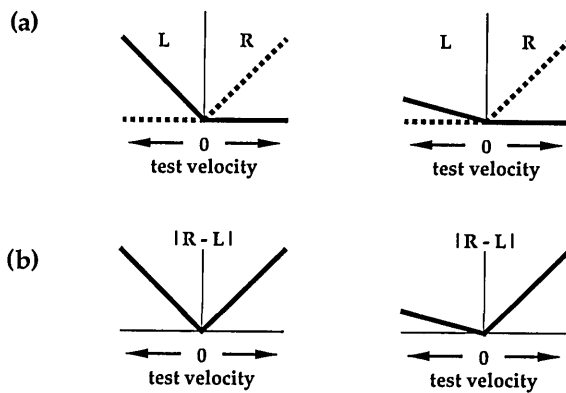


Fig. 8. Model that is reasonable but that nevertheless does not produce responses consistent with the experimental data. Left column, preadaptation responses; right column, postadaptation responses. (a) Leftward- and rightward-sensitive channels respond only to motion in their preferred direction. Following adaptation with a stimulus moving to the left, only the response of the L channel is reduced. (b) The absolute value of the opponent response is symmetric around zero velocity before adaptation. Following adaptation, the curve opens to the left and the minimum remains at zero velocity, which is contrary to the experimental results.

the combination stage could also produce similar results, though we have not explored the details of the elaborations needed to fit the data.

## 6. MODEL OF SIZE EFFECTS IN MOTION ADAPTATION

In this section we present a model that can account for the results of Experiment 3, in which we measured contrast thresholds for moving gratings of different vertical extent before and after motion adaptation. Thresholds for short tests were elevated more following adaptation with short fields than with taller fields. Tall adapting fields did elevate thresholds for tall fields. In other words, threshold elevation was maximal when the sizes of the adapting and test fields were the same. Models of early motion-sensing mechanisms<sup>34-36</sup> generally sum inputs linearly over their spatial receptive fields. Therefore a tall adapting stimulus should adapt individual units at least as much as a short adapting stimulus. In order to explain the experimental results, which suggest that a size match between adapting and test stimuli elevates thresholds maximally, some form of spatial interaction across motion-sensing mechanisms must be invoked. In the discussion of Experiment 3 (Subsection 4.D) we gave a verbal description of a system of inhibitory connections among motion-sensing units that would explain the experimental results. The model described in this section is intended as a demonstration that diffuse inhibitory mechanisms possess the properties necessary for generating results similar to the experimental data. Thus the fact that threshold elevation is maximal when adapting and test sizes match need not be due to hard-wired size-tuned units. The model is purposely kept very simple.

The basic structure of motion-sensing mechanisms is identical to that described for the model in Section 5 and shown in Fig. 4. We assume that visual space is tiled with the receptive fields of such mechanisms. In order to account for size-dependent adaptation phenomena, we

assume that mechanisms sampling different regions of visual space interact through inhibitory connections. Inhibition occurs independently for each direction-selective channel and before the gain-control stage. This inhibitory interaction takes place only for mechanisms with the same preferred direction of motion and is restricted to mechanisms along an axis orthogonal to the preferred direction. Figure 9 shows a schematic of the proposed interaction. Three motion-sensing units tuned to motion along the horizontal direction are shown distributed along the vertical axis. Dashed lines indicate inhibitory connections, with arrows showing the direction of the inhibitory signal. A dash inside a circle represents the summed inhibitory inputs received by a mechanism, as shown in the bottom unit, which receives inhibitory inputs from its nearest neighbor and from a unit that is further away in visual space. Not all connections are shown in the diagram; in fact, all mechanisms receive inhibitory inputs from all other mechanisms along the vertical axis. Thus all connections are reciprocal, as shown for the bottom and middle units. Each mechanism receives inhibition before the gain-control stage but after the stage that sends out the inhibitory output from that mechanism. Therefore the inhibitory output signal is not affected by inhibitory input from surrounding units; this simplifies the model analytically.

Inhibitory connections are given one further property: the strength of inhibition decreases as the separation between units in visual space increases. Figure 10 shows a schematic of an array of receptive fields tuned to leftward motion, with the remainder of the model not shown. A stimulus moving to the left, shown in Fig. 10(a), covers the array of receptive fields so that all mechanisms respond with equal magnitude. Units outside the region of the stimulus are not shown, since their output is zero. In the model, we have chosen a Gaussian as the spatial weighting

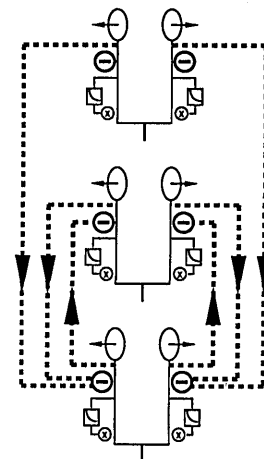


Fig. 9. Schematic of inhibitory connections among motion-sensing mechanisms. (a) Inhibition occurs independently for L and R channels, which are shown schematically as ellipses with inscribed arrows indicating their preferred direction of motion. Inhibitory connections are shown as dashed lines. Inhibition takes place among units along an axis orthogonal to the preferred direction of motion. A dash inside a circle represents the summed inhibitory inputs received by a mechanism, as shown in the bottom unit, which receives inhibitory inputs from its nearest neighbor and from the top unit. Not all connections are shown in the diagram; all connections are in fact reciprocal, as shown for the middle and bottom units.

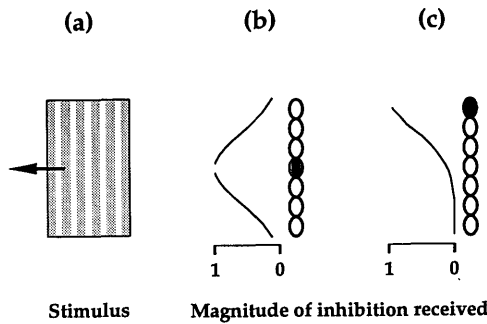


Fig. 10. Inhibitory inputs from spatiotemporal filters are weighted by distance in visual space. Ellipses represent receptive fields of filters tuned to leftward motion. The remainder of the model is not shown. For simplicity, receptive fields do not overlap. (a) The stimulus consists of a vertical grating at 100% contrast moving leftward. (b) All filters completely covered by the stimulus respond with equal magnitude. Filters not exposed to the stimulus are silent. The curve shows the magnitude of the inhibitory signal received by the shaded unit from surrounding units. Signals from nearby units are given a greater weight than inhibitory signals from units farther away in visual space. The gap at the peak of the curve indicates that units do not inhibit themselves. The total inhibitory signal is the weighted sum of inhibitory inputs from surrounding units. (c) The shaded unit near the edge of the moving stimulus receives less inhibition, since signals from units that are far removed are given only a small weight.

function for the inhibitory effect of surrounding units. The Gaussian shown in Fig. 10(b) indicates the amount of inhibition received by the shaded unit from the corresponding surrounding units. The break at the peak of the curve indicates that units do not inhibit themselves. The shaded unit receives more inhibitory input from nearby units than from units that are farther away. Figure 10(c) shows that the shaded unit near the border of the uniformly moving stimulus has fewer active neighbors and therefore receives a lesser amount of inhibition than does a unit near the center.

To simplify calculations, we assumed that the receptive fields of motion-sensing units do not overlap and that at the border of a moving stimulus no receptive field is only partially covered. In this way, the responses of all units exposed to the stimulus are the same, while all units outside the region covered by the stimulus are silent.

Next we describe the equations characterizing a motion-sensing unit that receives inhibitory input from other units as well as the particulars of manipulating the contrast instead of the velocity of a stimulus. Figure 11 shows a schematic of a motion-sensing unit. The outputs of spatiotemporal filters tuned to opposite directions of motion are labeled L and R in Fig. 11(a). Figure 11(e) shows the responses of these filters to optimally oriented gratings at 100% contrast moving at different velocities. We assumed that mechanisms were tuned to 5 Hz, with a standard deviation  $\sigma_{\text{mech}} = 3$  Hz. In Experiment 3, both adapting and test stimuli moved at a rate of 5 Hz. Therefore in the model we consider only the responses of the L and R mechanisms to tests moving at 5 Hz, which are labeled  $L_t$  and  $R_t$  in Fig. 11(e). In this simple model we assume that the response of a mechanism is linear with contrast. This is not a property of the "motion energy" filters described by Adelson and Bergen<sup>36</sup> but may be a justifiable assumption around threshold contrast. In this

way the responses of the L and R mechanisms for stimuli of different contrast will simply be scaled versions of those shown in the diagram. For stimuli moving leftward at 5 Hz, the responses of the L and R mechanisms are defined as follows:

$$L = \text{contrast} * L_t, \quad L_t = 1, \quad (9)$$

$$R = \text{contrast} * R_t, \quad R_t < 1, \quad (10)$$

where  $0 \leq \text{contrast} \leq 1$ . The inhibitory output signals, which are not shown in the diagram, branch off at this point and are equal to L and R. The inhibitory input signals are shown schematically in Fig. 11(b). The inhibi-

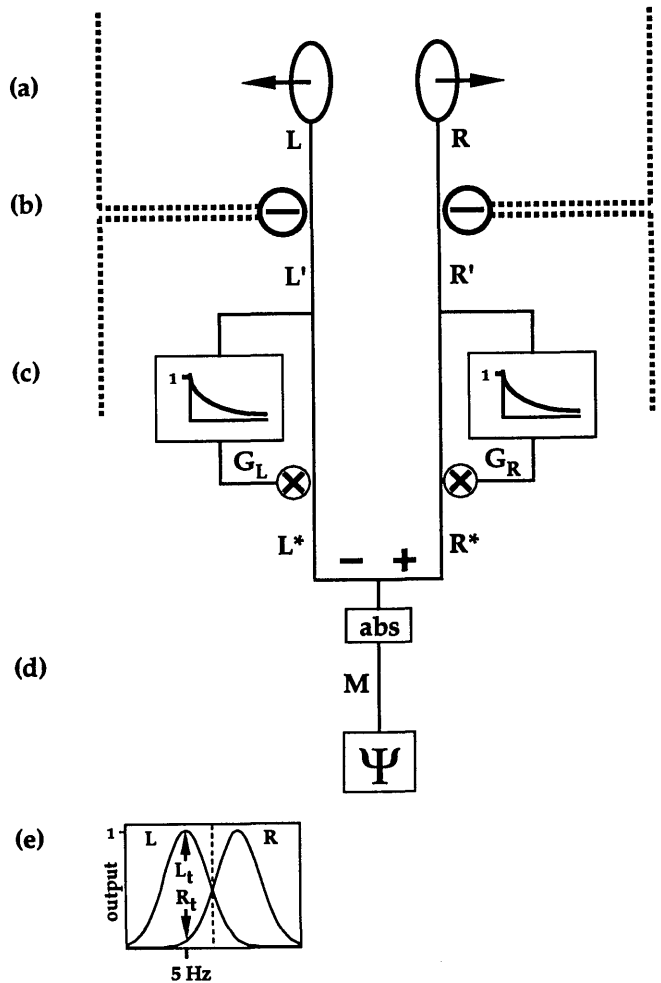


Fig. 11. Schematic of a motion-sensing unit that receives inhibitory inputs. (a) L, R, Outputs of spatiotemporal filters tuned to opposite directions of motion. The inhibitory output signals branch off at this point but are not shown in the diagram. The responses of the L and R channels to stimuli at different velocities are shown in (e), below the diagram.  $L_t, R_t$ , Responses of the two channels to test stimuli moving leftward at 5 Hz. As a simplification around contrast thresholds, we assume that the responses for the L and R channels scale linearly with the contrast of the test stimulus. (b) Summed inhibitory input and before the gain-control stage. Inhibitory input is subtracted from the L and R channels; the ensuing signals are labeled  $L'$  and  $R'$ . (c)  $G_L, G_R$ , Independent gain control for the left and right channels, respectively. Signals  $L'$  and  $R'$  are multiplied by the corresponding gain factors to generate  $L^*$  and  $R^*$ , respectively. (d) The absolute value of the opponent response,  $M$ , is passed through the Quick psychometric function to generate a probability of detection.

tory signals are simply subtracted from  $L$  and  $R$ ; the responses after the inhibitory input are  $L'$  and  $R'$  and are defined as follows:

$$L' = L - \sum_{i=1}^N \left( L_i * b * \exp \left\{ -\frac{1}{2} * \left[ \frac{\text{distance}(i)}{\sigma_{\text{inhib}}} \right]^2 \right\} \right), \quad (11)$$

$$R' = R - \sum_{i=1}^N \left( R_i * b * \exp \left\{ -\frac{1}{2} * \left[ \frac{\text{distance}(i)}{\sigma_{\text{inhib}}} \right]^2 \right\} \right). \quad (12)$$

$N$  is the number of units in the array. The strength of inhibitory outputs of surrounding motion-sensing mechanisms is described by  $L_i$  and  $R_i$ . The efficacy of these inhibitory outputs is then modified by the spatial weighting function described by the Gaussian. Units can be numbered, and the distance is simply the difference between the index of the unit receiving inhibition and the index of a given inhibitory unit. Since units do not inhibit themselves, a distance of zero is not considered. The spatial extent of inhibitory interactions is determined by  $\sigma_{\text{inhib}}$ . The term  $b$  weights all inhibitory inputs equally and is used to control the total magnitude of inhibition received by a mechanism. In the case in which the total magnitude of inhibition is greater than the excitation of a unit, we assume that the resulting response is rectified to zero.

The responses  $L'$  and  $R'$  are multiplied by the gain factors  $G_L$  and  $G_R$ , respectively, which arise in the gain control stage shown in Fig. 11(c). The gain functions are defined as

$$G_L = \frac{k}{k + (L')^p}, \quad (13)$$

$$G_R = \frac{k}{k + (R')^p}, \quad (14)$$

where  $k$  is the gain constant. The exponent  $p$  gives added control over the behavior of the gain function. Before adaptation, contrast = 0, so that  $G_L = G_R = 1$ . The contrast of the adapting stimulus was set equal to one; one calculates the gain factors for the postadaptation condition by using that value for the contrast. We assume that the adapting stimulus is presented for a long enough period for adaptation to reach a steady state in the gain function and that tests are short enough that the state of adaptation is not significantly altered.

The responses that have been modified by the gain factors are termed  $L^*$  and  $R^*$  and are defined as

$$L^* = L' * G_L, \quad (15)$$

$$R^* = R' * G_R. \quad (16)$$

The final output of motion-sensing mechanisms is the absolute value of the difference between the  $L^*$  and the  $R^*$  signals, which are then fed into the Quick psychometric function [Eq. (8)]. In this model we assume that contrast thresholds for the detection of moving gratings are dependent on the opponent signal. Experimental evidence shows that, for luminance stimuli, detection and motion thresholds are the same for the range 2–8 Hz.<sup>49</sup> Thus we can safely assume that the stimulus is seen as moving at contrast threshold, so that, in the model, detection threshold is the value of contrast for which the opponent-motion signal reaches some criterion value.

Next we describe the response of an array of motion-sensing units that interact through inhibitory connections when exposed to tall and short leftward-moving stimuli. The particular parameter settings used to produce the results that follow were  $k = 0.2955$ ,  $p = 0.1139$ ,  $b = 0.3623$ ,  $\sigma_{\text{inhib}} = 1.5$ ,  $N = 13$ .

Figure 12(a) shows a schematic of the stimulus that consists of a tall grating at 100% contrast moving leftward at 5 Hz. The output of the array of 13 mechanisms that is completely covered by this stimulus is shown in Figure 12(b). We consider only one column of units, whose location is plotted along the vertical axis. The output of each unit is plotted along the horizontal axis. Responses of the L channels are shown as asterisks; those of R channels as O's. The dashed curve shows the difference between responses of the L and the R channels. Units near the center of the stimulus receive more inhibition, so that output is less than for units near the edges. Varying contrast would simply scale this pattern of responses by the corresponding factor. The outputs of units near the center are not zero.

We assume that detection threshold is determined by probability summation of the opponent outputs of all units. Contrast threshold for a tall field is determined mainly by the output of the units near the edges, because those have the greatest output. Following adaptation with a tall grating, the response of each unit to the adapting stimulus, shown in Fig. 12(b), determines the gain factor, shown in Fig. 12(c). When a tall grating is used as a test [Fig. 12(d)], the preadaptation output is the same as the response to the adapting grating [Fig. 12(e)]. Following adaptation, the output of each unit is multiplied by the corresponding value in Fig. 12(c). The output of each unit after adaptation is shown in Fig. 12(f) as the response to a tall grating at 100% contrast: responses of all units are reduced. Thus a tall grating becomes less easily detectable following adaptation with a grating of the same size. We show responses only to leftward tests. The overall pattern of excitation for rightward tests would be similar, except that the magnitude of adaptation would not be as pronounced following a leftward adapting stimulus.

Next we consider the effects of adapting and testing with a short grating moving leftward. In the model we assume that a short test covers exactly one motion-sensing mechanism [Fig. 13(a)], so that the output of that mechanism is equal to one when the test grating is at 100% contrast, as shown in Fig. 13(b). Outputs of the surrounding units are zero. As a result of the large output during adaptation, the gain factor for the L channel, shown as an asterisk [Fig. 13(c)], is greatly reduced. Response to a short test stimulus [Fig. 13(d)] is therefore greatly reduced following adaptation [Fig. 13(f)]. This makes the grating much less easily detectable.

When adapting with a tall grating [Fig. 14(a)], outputs of units near the center of the grating are small (14b), which leads to a gain value near one [Fig. 14(c)]. A short test [Fig. 14(d)] elicits a response only from the unit in the center of the array [Fig. 14(e)]. Following adaptation with a tall grating, the response of the unit exposed to the short test, shown in Fig. 14(f), is reduced less than in Fig. 13(f). Postadaptation thresholds would therefore not be elevated as much as after adaptation to a short grating.

In Fig. 15 we show results generated by this model that

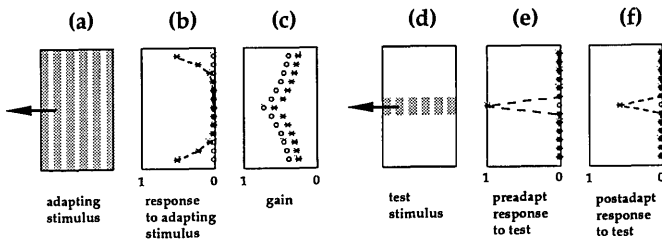


Fig. 12. Responses of motion-sensing units to tall adapting and test stimuli. All gratings are assumed to be optimal for the spatiotemporal filters. Gratings are at 100% contrast, which elicits a response equal to one. (a) Tall adapting stimulus. (b) Motion-sensing units are distributed along the vertical axis. Responses to the adapting stimulus are plotted along the horizontal axis. \*, Responses of L channels; O, responses of R channels. Dashed curve, difference between L and R channels. The smallest response shown is not zero. (c) Gain factor for L and R channels. Symbols correspond to those used in (b). (d) Tall test stimulus. (e) Preadaptation responses of L and R channels. (f) Postadaptation responses of channels.

inhibition across units take place before the gain-control stage. O'Shea and Rowell<sup>50</sup> measured electrical activity of the lobular giant movement detector in the locust. The response to a small moving target was diminished when a moving surround was added to the image. Response increased as the surround was moved farther away from the small target. This property is consistent with a lateral inhibitory network. Furthermore, the response to a small target was diminished after repeated presentations of the stimulus. When the small moving target was surrounded by a large moving field, the response did not diminish with multiple presentations. The data suggest that lateral inhibition helps to prevent adaptation to large-field mo-

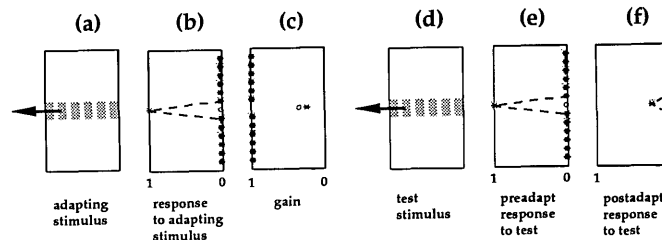


Fig. 13. Responses of motion-sensing units to short adapting and test stimuli. (a) Short adapting stimulus. (b) Only one motion-sensing unit is covered by the stimulus. Surrounding units are silent. (c) Gain factor for the unit that responds to the adapting stimulus. Gains for other units are equal to one. (d) Short test stimulus. (e) Preadaptation response of the unit exposed to the stimulus. (f) Postadaptation response.

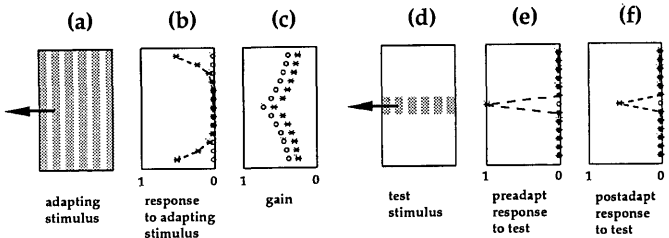


Fig. 14. Responses of motion-sensing units to tall adapting stimuli and short test stimuli. (a) Tall adapting stimulus. (b) Response to adapting stimulus. (c) Gain factor for each unit. (d) Short test grating. (e) Response of L and R channels to a short test grating before adaptation. (f) Response to a short test grating following exposure to a tall adapting grating. The response is greater than in Fig. 13(f).

correspond to the experimental conditions described in Experiment 3. For every condition shown in Figs. 12-14, opponent outputs of all active units were pooled in the Quick psychometric function to generate a probability of detection. Contrast was varied until the probability of detection was 80%, which was the value tracked by the staircase procedure in Experiment 3. The model's parameters were set so that preadaptation thresholds had the same values as the experimental results for observer WLS, with 0.4-cycle/deg gratings ( $m = 0.0037$ ,  $\alpha = 0.8789$ ). Indices for total desensitization and directional desensitization were calculated as in Experiment 3 and are plotted as open circles and filled squares, respectively. The results can be compared with the experimental data in Fig. 3. The modeling results are qualitatively similar to the experimental results: desensitization indices were greater when adapting and test sizes were the same than when the test was smaller than the adapting field.

We have shown that a simple model involving diffuse inhibitory interactions among motion-sensing mechanisms has properties that mimic experimental results. Thus size-dependent adaptation need not be based on hard-wired size-tuned units. The example described here serves merely to illustrate one implementation of the model. The central idea simply requires that diffuse

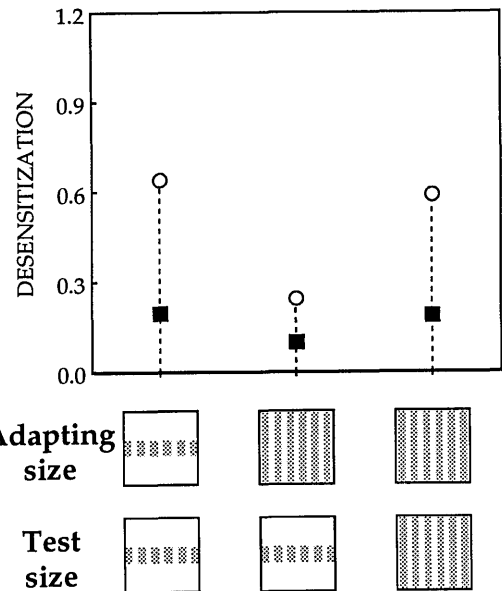


Fig. 15. Contrast thresholds generated by the model for the conditions shown in Figs. 12-14. Opponent outputs of all active units were pooled in the Quick psychometric function to generate a probability of detection. Contrast was varied until the probability of detection reached 80%. Parameters were set so that preadaptation thresholds had the same values as results for 0.4-cycle/deg gratings in Experiment 3 for observer WLS. Indices for total desensitization and directional desensitization were calculated as in Experiment 3 and are plotted as open circles and filled squares, respectively. Schematics of the adapting and testing conditions are shown on the abscissa. For parameter settings, see text.

tion. The model that we present to explain size-dependent effects in adaptation uses a similar principle.

## 7. SUMMARY

In this study we have addressed two main issues: (1) we tested a measure of the effect of prolonged exposure to moving stimuli on subsequent perception of motion and (2) we explored spatial properties of the processing of moving stimuli by comparing adaptation magnitudes for different size combinations of adapting and test stimuli. In Experiment 1 we measured psychometric curves for the detection of motion of briefly presented stimuli. Following motion adaptation, the psychometric curve was shifted with respect to the preadaptation curve, and at the minimum the probability of detection was no longer zero. The changes in the psychometric curve put constraints on the types of model that can be invoked to explain the motion aftereffect. To explain the experimental data, we presented a model that consists of independent motion-sensing mechanisms tuned to different rates of motion and incorporating multiplicative gain controls before the opponent stage. In Experiment 2 we measured psychometric curves for the detection of motion of a short stimulus following adaptation with a tall stimulus. The postadaptation psychometric curve was displaced less from the origin than when the adapting and the test stimuli were the same size. We corroborated the results of Experiments 1 and 2 in Experiment 3 by measuring contrast thresholds for the detection of moving stimuli. In addition, we varied the sizes of adapting and test stimuli, and results indicate that adaptation magnitude is greatest when adapting and test sizes match. We proposed a model that invokes diffuse inhibitory connections among motion-sensing mechanisms and showed that it possesses properties that are reflected in the experimental results. Thus hard-wired size-tuned mechanisms are not required for explanation of experimental results that exhibit size-dependent adaptation.

## ACKNOWLEDGMENTS

We thank Sean Daly for patient and careful observation in a demanding experiment. This research was partially supported by the National Eye Institute through grant EY07556 to Q. Zaidi. Portions of this research were presented at the meeting of the Association for Research in Vision and Ophthalmology (1990).

## REFERENCES

1. A. Wohlgenuth, "On the aftereffect of seen movement," *Br. J. Psychol. Monogr. Suppl.* **1**, 1-117 (1911).
2. H. C. Holland, *The Spiral Aftereffect* (Pergamon, London, 1965).
3. S. Anstis, "Motion perception in the frontal plane. Sensory aspects," in *Handbook of Perception and Human Performance*, K. R. Boff, L. Kaufman, and J. P. Thomas, eds. (Wiley, New York, 1986), Vol. I.
4. R. Sekuler and A. Pantle, "A model for after-effects of seen movement," *Vision Res.* **7**, 427-439 (1967).
5. M. M. Taylor, "Tracking the decay of the after-effect of seen rotary movement," *Percept. Mot. Skills* **16**, 119-129 (1963).
6. M. J. Keck, T. D. Palella, and A. Pantle, "Motion aftereffect as a function of the contrast of sinusoidal gratings," *Vision Res.* **16**, 187-191 (1976).
7. A. Pantle, "Motion aftereffect magnitude as a measure of the spatio-temporal response properties of direction-selective analyzers," *Vision Res.* **14**, 1229-1236 (1974).
8. W. J. Lovegrove, R. Over, and J. Broerse, "Colour selectivity in motion after-effect," *Nature (London)* **238**, 334-335 (1972).
9. O. E. Favreau, V. F. Emerson, and M. C. Corballis, "Motion perception: a color-contingent aftereffect," *Science* **176**, 78-79 (1972).
10. K. T. Mullen and C. L. Baker, Jr., "A motion aftereffect from an isoluminant stimulus," *Vision Res.* **25**, 685-688 (1985).
11. J. E. W. Mayhew and S. M. Anstis, "Movement aftereffects contingent on color, intensity, and pattern," *Percept. Psychophys.* **12**, 77-85 (1972).
12. A. M. Derrington and D. R. Badcock, "The low level motion system has both chromatic and luminance inputs," *Vision Res.* **25**, 1879-1884 (1985).
13. P. Cavanagh and O. E. Favreau, "Color and luminance share a common motion pathway," *Vision Res.* **25**, 1595-1601 (1985).
14. A. Pantle, "Adaptation to pattern spatial frequency: effects on visual movement sensitivity in humans," *J. Opt. Soc. Am.* **60**, 1120-1124 (1970).
15. D. J. Tolhurst, "Adaptation to square-wave gratings: inhibition between spatial frequency channels in the human visual system," *J. Physiol. (London)* **226**, 231-248 (1972).
16. C. R. Sharpe and D. J. Tolhurst, "Orientation and spatial frequency channels in peripheral vision," *Vision Res.* **13**, 2103-2112 (1973).
17. D. J. Tolhurst, "Separate channels for the analysis of the shape and the movement of a moving visual stimulus," *J. Physiol. (London)* **231**, 385-402 (1973).
18. R. W. Sekuler, E. L. Rubin, and W. H. Cushman, "Selectivities of human visual mechanisms for direction of movement and contour orientation," *J. Opt. Soc. Am.* **58**, 1146-1150 (1968).
19. C. R. Sharpe and D. J. Tolhurst, "The effects of temporal modulation on the orientation channels of the human visual system," *Perception* **2**, 23-29 (1973).
20. C. F. Stromeyer III, R. E. Kronauer, and J. C. Madsen, "Opponent-movement mechanisms in human vision," *J. Opt. Soc. Am. A* **1**, 876-884 (1984).
21. E. Levinson and R. Sekuler, "The independence of channels in human vision selective for direction of movement," *J. Physiol. (London)* **250**, 347-366 (1975).
22. E. Levinson and R. Sekuler, "Inhibition and disinhibition of direction-specific mechanisms in human vision," *Nature (London)* **254**, 692-694 (1975).
23. D. J. Tolhurst, C. R. Sharpe, and G. Hart, "The analysis of the drift rate of moving sinusoidal gratings," *Vision Res.* **13**, 2545-2555 (1973).
24. M. Green, "Psychophysical relationship among mechanisms sensitive to pattern, motion and flicker," *Vision Res.* **21**, 971-983 (1981).
25. S. M. Anstis and A. H. Reinhardt-Rutland, "Interactions between motion aftereffects and induced movement," *Vision Res.* **16**, 1391-1394 (1976).
26. C. Bonnet and V. Poutahs, "Interactions between spatial and kinetic dimensions in movement aftereffect," *Percept. Psychophys.* **12**, 193-200 (1972).
27. K. Nakayama and D. J. Roberts, "Line length detectors in the human visual system: evidence from selective adaptation," *Vision Res.* **12**, 1709-1713 (1972).
28. G. Westheimer, "Eye movement responses to a horizontally moving visual stimulus," *Arch. Ophthalmol. (Chicago)* **52**, 932-941 (1954).
29. G. C. Grindley and R. T. Wilkinson, "The aftereffect of seen movement on a plain field," *Q. J. Exper. Psychol.* **5**, 183-184 (1953).
30. M. Green, M. Chilcoat, and C. F. Stromeyer III, "Rapid motion aftereffect seen within uniform flickering test fields," *Nature (London)* **304**, 61-62 (1983).
31. C. H. Graham, *Vision and Visual Perception* (Wiley, New York, 1965).
32. R. Cords and E. T. v. Bruecke, "Ueber die Geschwindigkeit des Bewegungsnachbildes," *Pfluegers Arch. Ges. Physiol.* **119**, 54-76 (1907).
33. R. G. Bennett and G. Westheimer, "A shift in the perceived simultaneity of adjacent visual stimuli following adaptation

- to stroboscopic motion along the same axis," *Vision Res.* **25**, 565-569 (1985).
34. J. P. H. van Santen and G. Sperling, "Elaborated Reichardt detectors," *J. Opt. Soc. Am. A* **2**, 300-321 (1985).
  35. A. B. Watson and A. J. Ahumada, Jr., "Model of human visual-motion sensing," *J. Opt. Soc. Am. A* **2**, 322-342 (1985).
  36. E. H. Adelson and J. R. Bergen, "Spatiotemporal energy models for the perception of motion," *J. Opt. Soc. Am. A* **2**, 284-299 (1985).
  37. R. W. Sekuler and L. Ganz, "Aftereffect of seen motion with a stabilized retinal image," *Science* **139**, 419-420 (1963).
  38. A. J. Pantle and R. W. Sekuler, "Velocity-sensitive elements in human vision: initial psychophysical evidence," *Vision Res.* **8**, 445-450 (1968).
  39. T. Cornsweet, "The staircase method in psychophysics," *Am. J. Psychol.* **75**, 485 (1962).
  40. Q. Zaidi and W. L. Sachtler, "Motion adaptation from surrounding stimuli," *Perception* **20**, 703-714 (1992).
  41. N. S. Sutherland, "Figural after-effects and apparent size," *Q. J. Exper. Psychol.* **13**, 222-228 (1961).
  42. A. B. Clymer, "The effect of seen motion on the apparent speed of subsequent test velocities: speed tuning of movement," Ph.D. dissertation (Columbia University, New York, 1973).
  43. P. Thompson, "Velocity after-effects: the effect of adaptation to moving stimuli on the perception of subsequently seen moving stimuli," *Vision Res.* **21**, 337-345 (1981).
  44. R. C. Emerson, J. R. Bergen, and E. H. Adelson, "Directionally selective complex cells and the computation of motion energy in cat visual cortex," *Vision Res.* **32**, 203-218 (1992).
  45. R. F. Quick Jr., "A vector-magnitude model of contrast detection," *Kybernetik* **16**, 65-67 (1974).
  46. D. H. Hubel and T. N. Wiesel, "Receptive fields and functional architecture in two nonstriate visual areas (18 and 19) of the cat," *J. Neurophysiol.* **28**, 229-289 (1965).
  47. G. A. Orban, H. Kennedy, and H. Maes, "Response to movement of neurons in areas 17 and 18 of the cat: velocity sensitivity," *J. Neurophysiol.* **45**, 1043-1058 (1981).
  48. J. H. R. Maunsell and D. C. Van Essen, "Functional properties of neurons in middle temporal visual area of the macaque monkey. I. Selectivity for stimulus direction, speed, and orientation," *J. Neurophysiol.* **49**, 1127-1147 (1983).
  49. P. Cavanagh, "The contribution of color to motion," in *From Pigments to Perception. Advances in Understanding Visual Processes*, A. Valberg and B. B. Lee, eds., Vol. 203 of NATO ASI Series, Series A: Life Sciences (Plenum, New York, 1991), pp. 151-164.
  50. M. O'Shea and C. H. F. Rowell, "Protection from habituation by lateral inhibition," *Nature (London)* **254**, 53-55 (1975).